https://doi.org/10.1038/s44303-026-00138-x

Accelerated and localized synucleinopathy in a hybrid mouse model: implications for positron emission tomography studies

Chunfang A. Xia[1] ✉, Hsiu-Ming Tsai[1], Sandra Diaz Garcia[2], Shuanglong Liu[3], Alessandra Matzeu[2], Mani Salarian[1], Wouter Bruinzeel[4] & Anna K. Szardenings[1]

Parkinson's disease (PD) is characterized by alpha-synuclein (α-syn) aggregation, dopaminergic (DA) neuron loss, and neuroinflammation. Synucleinopathy, the α-syn-related pathology, is the central to the pathogenetic processes observed in the brains of patients with PD, dementia with Lewy bodies (DLB), and multiple system atrophy (MSA). We are seeking an animal model with synucleinopathy that can comprehensively replicate these pathologies and adhere to suitable timeframes for preclinical research for positron emission tomography (PET) imaging studies. Adeno-associated virus (AAV) carrying the mutated human α-syn gene and S87N α-syn preformed fibrils (PFF) were co-injected into the left substantia nigra (SN) of mouse brains. Immunohistochemistry (IHC) and PET/CT imaging were performed at different time points to detect the key pathologies in the brain. This model resulted in accelerated α-syn pathology, detectable as early as two weeks post-injection, alongside DA neuron loss, microglial activation, reduced synaptic density, and impaired mitochondrial function within five weeks. Pathology remained spatially localized. In summary, this AAV/PFF hybrid model offers a rapid, region-specific platform for studying synucleinopathies such as PD, as well as for evaluating PET ligands for disease diagnosis and monitoring.

Parkinson's disease (PD) is a progressive synucleinopathy pathologically characterized by the presence of alpha-synuclein (α-syn) aggregation, loss of nigrostriatal dopaminergic (DA) neurons, neuroinflammation, and mitochondrial dysfunction, among other features[1]. As PD progresses, α-syn misfolds and aggregates, leading to the formation of Lewy bodies and Lewy neurites that spread through the brain in a prion-like manner[2,3]. Various studies have suggested that α-syn inclusion-induced toxicity is a major factor in DA neuron death[4]. Given the complex etiology and multifactorial nature of PD, understanding the disease mechanism and identifying an ideal disease model is crucial. The ideal PD model should include the following features[5,6]: 1. A loss of more than 50% of nigrostriatal DA neurons, easily detectable through biochemical and neuropathological techniques; 2. The presence and development of Lewy bodies as indicators of α-syn pathology; 3. Replication of disease progression over a short period of time, facilitating faster and more cost-effective screening of potential therapeutic candidates.

Rodent models of different forms of synucleinopathy have been developed using transgenic techniques, viral vector-mediated gene transferor, or inoculation with preformed fibrils (PFFs) seeds[7,8]. In transgenic mouse models, α-syn forms intracellular inclusions in many, but not all, α-syn-overexpressing transgenic mice[9]. The anatomical distribution of α-syn inclusions also varies widely among models, even among those with the same promoter[10]. While these models provide some insight into protein aggregation, they do not accurately replicate the progressive loss of DA neurons seen in patients. Over the past two decades, delivering α-syn using an adeno-associated virus (AAV) vector has become a flexible and effective method for creating models that closely replicate the brain changes seen in PD and other Lewy body disorders[11]. But in this model, the degenerative changes develop slowly, and substantial DA neuron cell loss is obtained only with very high expression levels[12]. Our previous study demonstrated that this model requires at least 4–5 months to develop a limited amount of α-syn

[1]Discovery Technologies and Molecular Pharmacology, Johnson & Johnson, San Diego, CA, USA. [2]Preclinical Sciences and Translational Safety, Johnson & Johnson, San Diego, CA, USA. [3]Global Discovery Chemistry, Johnson & Johnson, San Diego, CA, USA. [4]Neuroscience Discovery, Johnson & Johnson, Beerse, Belgium. ✉e-mail: cxia1@its.jnj.com

aggregates (see Supplementary Fig. 1). Additionally, the inflammatory response is transient and of modest magnitude. PFFs are recognized as seeds that promote the recruitment of monomeric α-syn into toxic fibrillar aggregates[13,14]. However, the aggregated α-syn in mice was of rodent form rather than human, and the rate of this aggregation process depends on the intracellular levels of α-syn. Thakur et al.[15] reported a combination of fibril seeds and α-syn overexpression in a rat model. The model replicates key features of human synucleinopathy, DA degeneration, impaired motor function, and inflammation. However, the model involves multiple surgeries: two AAV6-mediated α-syn vector injections into the substantia nigra (SN) and ventral tegmental area, followed by another two PFF injections 4 weeks later. This significantly increases the complexity of the procedure, making it challenging for researchers to replicate or standardize. Additionally, multiple surgeries cause further injury and stress to animals. Bjorklund et al. measured the combined SynFib model in rat and mouse models[16]. In their study, they observed α-syn overexpression and a loss of tyrosine hydroxylase (TH) at later time points post-injection—12 weeks in the mouse brain, 4 and 16 weeks in the rat model.

PET is a powerful imaging technique used to study brain function and pathology in PD[17]. By bridging the gap between clinical symptoms and underlying pathology, PET enables earlier interventions, enhances disease management, and supports the development of targeted therapies. Currently, PET imaging for PD primarily focuses on assessing dopamine transporter activity with [^{18}F]DOPA[18] and brain metabolism with [^{18}F]FDG[19] to identify disease-specific changes. Ongoing research aims to develop additional PET ligands capable of detecting pathological α-syn, neuroinflammation, and other pathological features. An ideal animal model for PET ligand development should exhibit significant α-syn pathology that closely resembles Lewy bodies or neurites, along with neuroinflammation and mitochondrial dysfunction, mirroring the pathologies observed in PD brains. Additionally, it should demonstrate regional and focal distributions of pathologies detectable by a PET tracer as well as temporal dynamics to allow for longitudinal studies corresponding to disease progression and ligand-binding evaluations.

To address these limitations and needs, we evaluated this hybrid model that provides a more accurate, focal, and comprehensive representation of PD, thereby facilitating PET ligand assessment. This model significantly accelerates α-syn pathology, observable as early as 2 weeks post-surgery, alongside DA neuron loss, microglial activation, reduced synaptic density, and impaired mitochondrial function at later time points. The localized injection induces focal pathologies development in the mouse brain, aligning well with the requirements for effective PET ligand development for PD.

Results

Pathological α-syn aggregation

A distinguishing feature of the AAV/PFF model is the early development of inclusions and aggregates of phospho-Ser129-synuclein (p-syn) in the affected nigral DA neurons. High levels of human α-syn expression were detected in mouse brains starting at 2 weeks post AAV/PFF injection (Fig. 1a). Human α-syn spread from the SN to most regions of the ipsilateral hemisphere. The p-syn was found to be more concentrated around the SN compared to total α-syn (Fig. 1a). Both α-syn monomer and p-syn densities showed an increasing trend from 2 to 5 weeks (Supplementary Fig. 2). Double staining showed colocalization of both markers (Fig. 1b). Lewy body-like p-syn pathology was observed in many neurons around the SN region (indicated by arrows), as well as in distorted axons and dendrites, resembling Lewy neurites (marked by arrowheads in Fig. 1b).

Dopaminergic neuron loss

Representative double staining for vesicular monoamine transporter 2 (VMAT2) and TH revealed significant DA neuron loss in the striatum as shown in Fig. 2a. The intensity of TH, measured by immunohistochemistry (IHC) in the striatum of injection side, demonstrated a gradual reduction

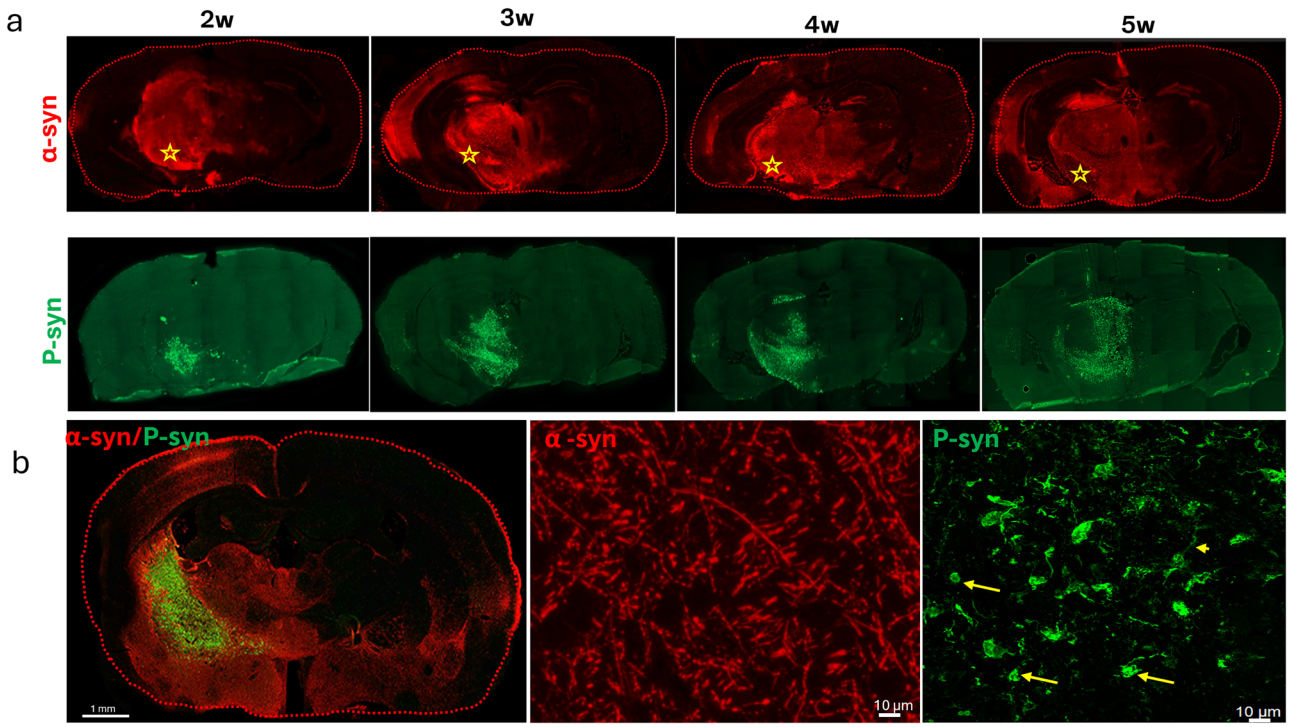

Fig. 1 | Human α-syn and p-syn expression in mouse brains from 2 to 5 weeks post-injection. Overexpression of human α-syn and p-syn IHC on coronal brain sections across SN (**a**). Yellow stars indicate the injection site. **b** Representative double immunostaining of α-syn and p-syn on mouse brain sections at 4 weeks post-injection. High magnification shows α-syn monomers (bottom middle). Lewy body-like (arrows) and Lewy neurite-like (arrowheads) structures can be found under a confocal microscope (bottom right).

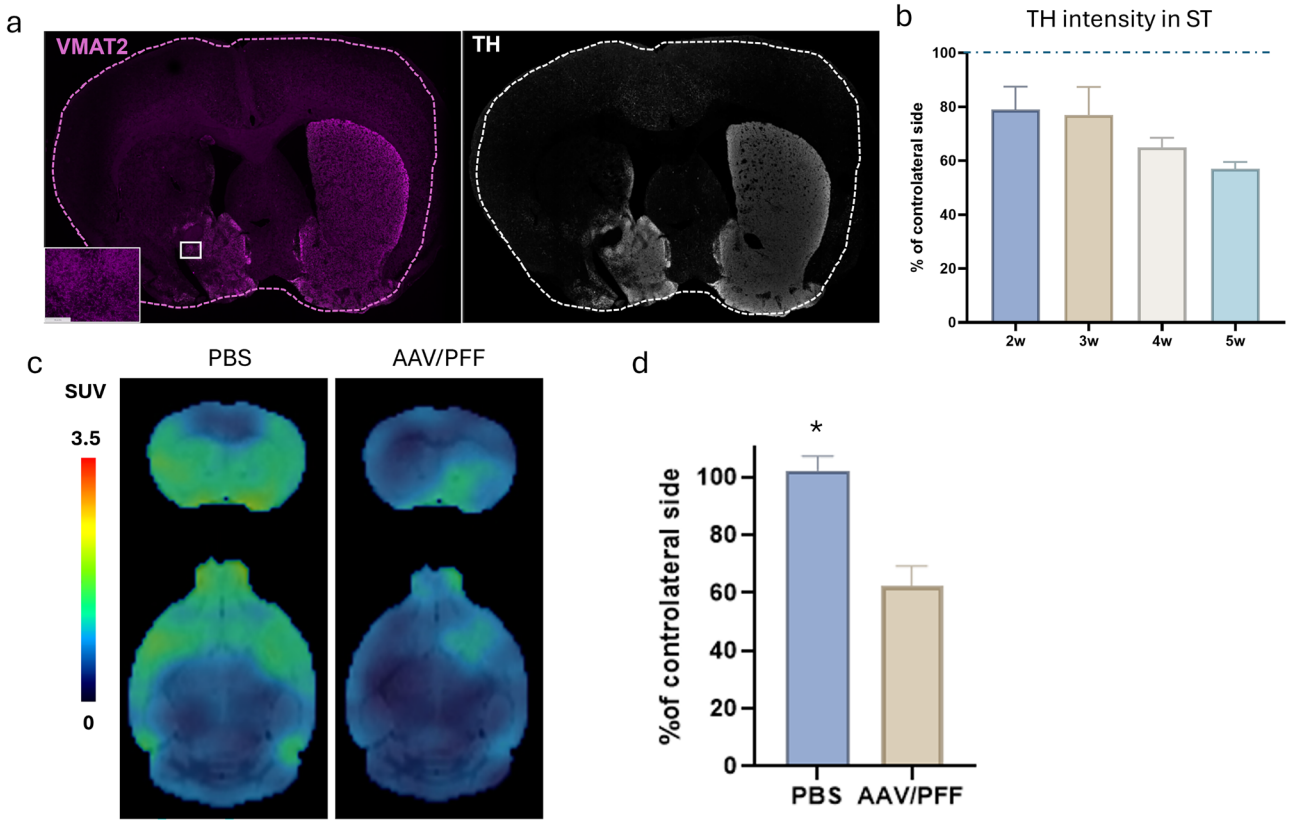

Fig. 2 | DA neuron degradation in the striatum. a Representative images of immunostaining of VMAT2 and TH on mouse brain sections across the striatum at 4 weeks post AAV/PFF injection. **b** DA neuron deficiency in the striatum was observed at all time points from 2 to 5 weeks ($n = 3$). **c** Comparison of VMAT2 PET imaging in the mouse brain at 4 weeks post-injection between PBS and AAV/PFF. **d** Percentage of uptake of contralateral sides ($n = 3$, $^*P < 0.005$).

over time post the injection (Fig. 2b). Specifically, TH intensity was measured at 79%, 77%, 65%, and 59% of contralateral side at 2, 3, 4, and 5 weeks post-injection, respectively (Fig. 2b, $n = 3$). Based on IHC, a PET/CT scan was conducted at 4 weeks post-injection. The axial and coronal PET images illustrated the patterns of brain uptake in both PBS and AAV/PFF groups using a VMAT2 tracer, [^{18}F]AV-133 (Fig. 2c). The uptake in the ipsilateral and contralateral striatum did not show significant differences with PBS injection. In contrast, the AAV/PFF mice displayed a decreased uptake on the ipsilateral side 4 weeks post-injection (Fig. 2c). A ~40% reduction in uptake was observed in the ipsilateral striatum compared to the contralateral side, as illustrated in Fig. 2d.

Neuroinflammation

A microglial reaction was detected by Iba1 staining, spreading from the ipsilateral SN to the midbrain and thalamus, from 2 to 5 weeks post-injection (Fig. 3a). Multiplex staining of p-syn, Iba1, and triggering receptor expressed on myeloid cells 2 (TREM2) provided clear evidence of inflammatory responses localized to regions with pathological p-syn deposits at 3 weeks post-surgery (Fig. 3b). The results showed that the inflammatory response expanded in correlation with the presence of pathological α-syn, demonstrating pronounced microglial activation in the affected areas. This sharply contrasts with the contralateral side of the brain, where such inflammatory markers were notably less prominent, and cellular morphology indicated non-reactive microglia (Fig. 3c).

Colony-stimulating factor 1 receptor (CSF1R), a marker of neuroinflammation primarily expressed by microglia in the central nervous system, exhibited increased expression in the presence of p-syn following AAV/PFF treatment and peaked at 3 weeks post-surgery, as illustrated in Supplementary Fig. 2. The small molecule PET ligand [^{18}F]JNJ-CSF1R-1 was used to target CSF1R and detect neuroinflammation[20,21]. CSF1R PET imaging revealed elevated uptake in the ipsilateral SN, indicating increased inflammation around the injection site. The uptake patterns identified in PET imaging were in good agreement with the IHC findings (Fig. 4b, c). Tracer uptake was quantified by comparing the ipsilateral region to its contralateral counterpart. PET analysis revealed that [^{18}F]JNJ-CSF1R-1 uptake at the injection site was 42% higher than on the contralateral side (Fig. 4e, $n = 3$, $P < 0.01$). IHC demonstrated a similar trend, with an average 49% increase (Fig. 4d, $n = 3$, $P < 0.05$). The elevated ipsilateral uptake indicates a significant focal increase in CSF1R radiotracer concentration, reflecting enhanced microglial activation.

Synapse integrity

Synaptic density at a later time (week 5) is measured by synaptic vesicle protein 2A (SV2A), which is considered a key marker for presynaptic density. SV2A IHC revealed a significant reduction in synaptic density around the ipsilateral SN area (Fig. 5a) at 5 weeks post-injection. Compared to the contralateral side of the brain, where synaptic integrity remained relatively intact (Fig. 5b). The PET images illustrate synaptic density patterns of brain uptake in both the PBS and AAV/PFF groups using the [^{18}F] UCB-H tracer, employing axial and coronal sections in Fig. 5c. Identical regions of interest (ROIs) were applied to both the PBS and AAV/PFF groups for evaluation. The uptake in the ipsilateral and contralateral sides did not show significant differences in the PBS group. In the AAV/PFF-treated group, an average 18% reduction in tracer uptake was observed in the ipsilateral SN compared to the contralateral side, but the difference is not significant ($n = 3$, $P > 0.05$, Fig. 5c).

Mitochondrial dysfunction

IHC of ATP synthase subunit A (ATP5A), a key mitochondrial marker, revealed a decrease in expression correlated with the extent of α-syn pathology observed at 5 weeks post-injection compared to the contralateral side (Fig. 6a, b). The PET imaging of [^{18}F] BCPP-EF tracer was

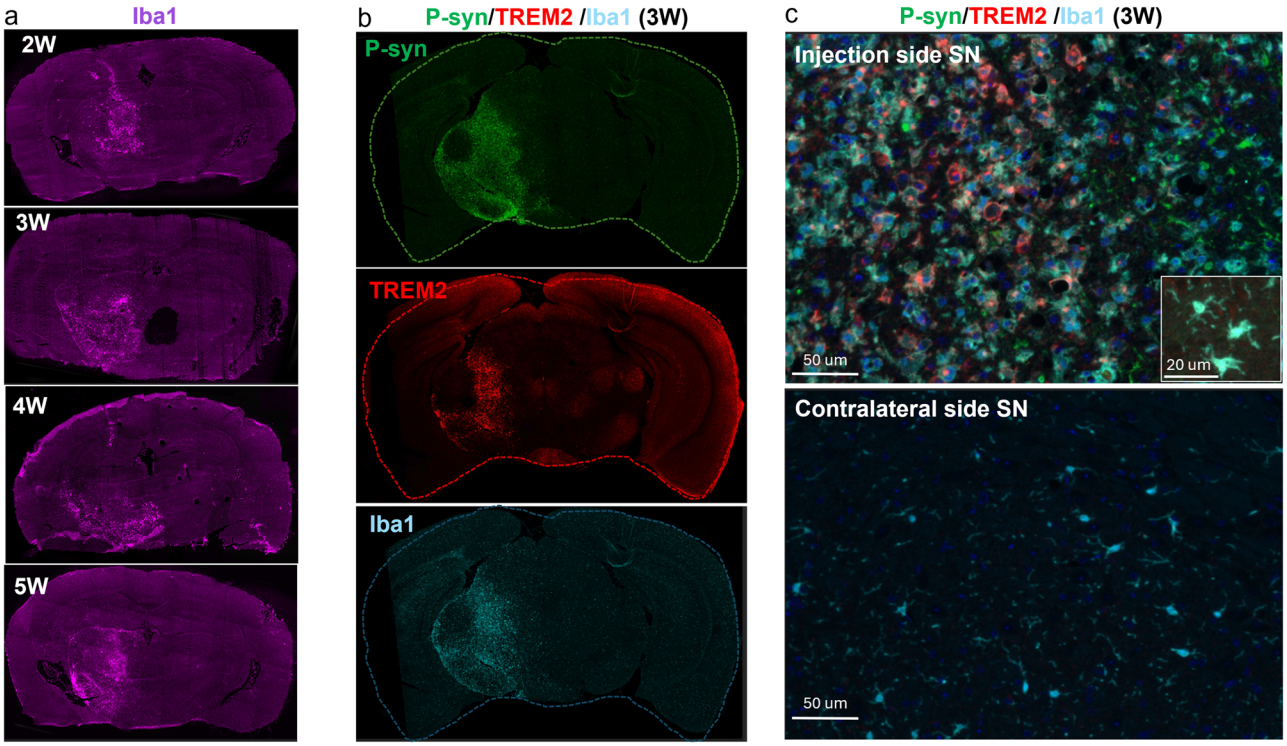

Fig. 3 | Neuroinflammation was colocalized with aggregated α-syn deposits. **a** Iba1 staining on mouse brain sections from 2 to 5 weeks post AAV/PFF injection. **b** Multiplex staining of p-syn, TREM2, and Iba1 IHC on mouse brain tissue collected 3 weeks post AAV/PFF injection. **c** Increased Iba1 and TREM2 protein expression levels were observed in regions with overexpressed p-syn. High-magnification imaging revealed microglial activation.

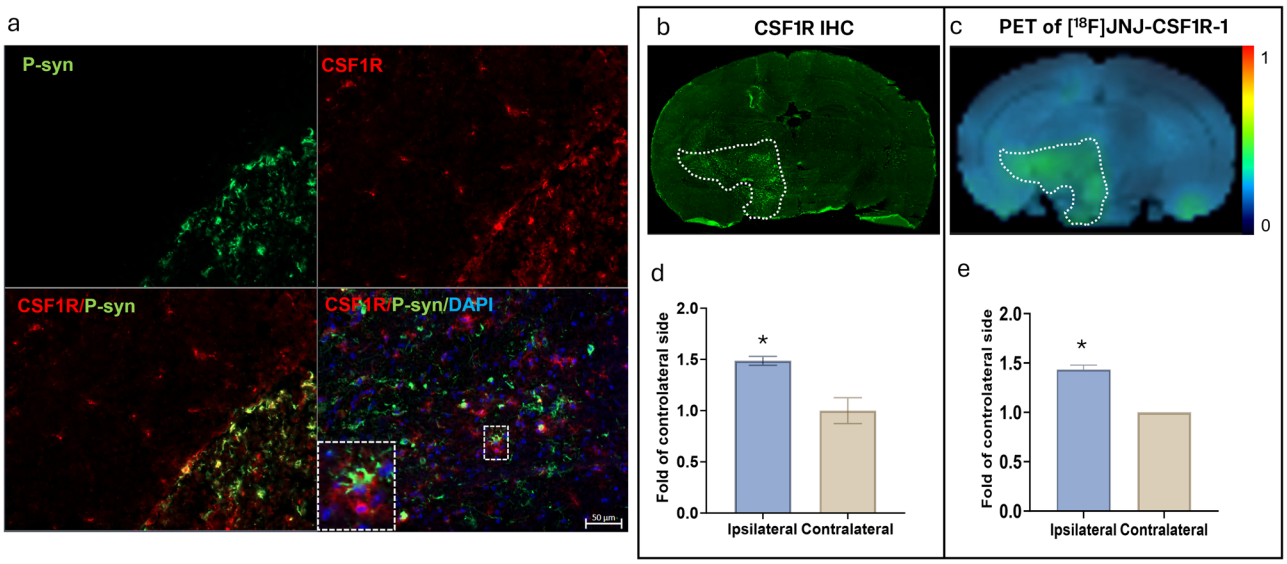

Fig. 4 | Increased CSF1R level measured by IHC and PET imaging. **a** IHC indicates that CSF1R levels increased with the presence of p-syn (scale bar = 50 μm). **b**, **c** In vivo PET signal of [^{18}F]JNJ-CSF1R-1 and CSF1R IHC was compared side-by-side in the same animal. The bar charts (**d**, **e**) illustrated the increased signal in the ipsilateral side compared to the contralateral side based on IHC and PET images ($n = 3$, $^{*}P < 0.05$).

used to analyze mitochondrial integrity in both the PBS and AAV/PFF groups (shown in Fig. 6c). The brain uptake in the ipsilateral and contralateral SN showed no significant differences in the PBS group, indicating preserved mitochondrial integrity. In contrast, the AAV/PFF group demonstrated a slight but significant reduction of 7.3% in uptake between the ipsilateral and contralateral SN ($n = 3$, $P < 0.01$), as depicted in Fig. 6c.

Discussion

Rodent models of synucleinopathy, such as PFF injections[22] or AAV-mediated α-syn overexpression (Supplementary Fig. 1), develop pathology slowly and show only minimal changes in key features over time. In contrast, the hybrid AAV/PFF model introduced in this study is specifically designed to address these limitations, making it exceptionally suitable for PET imaging applications.

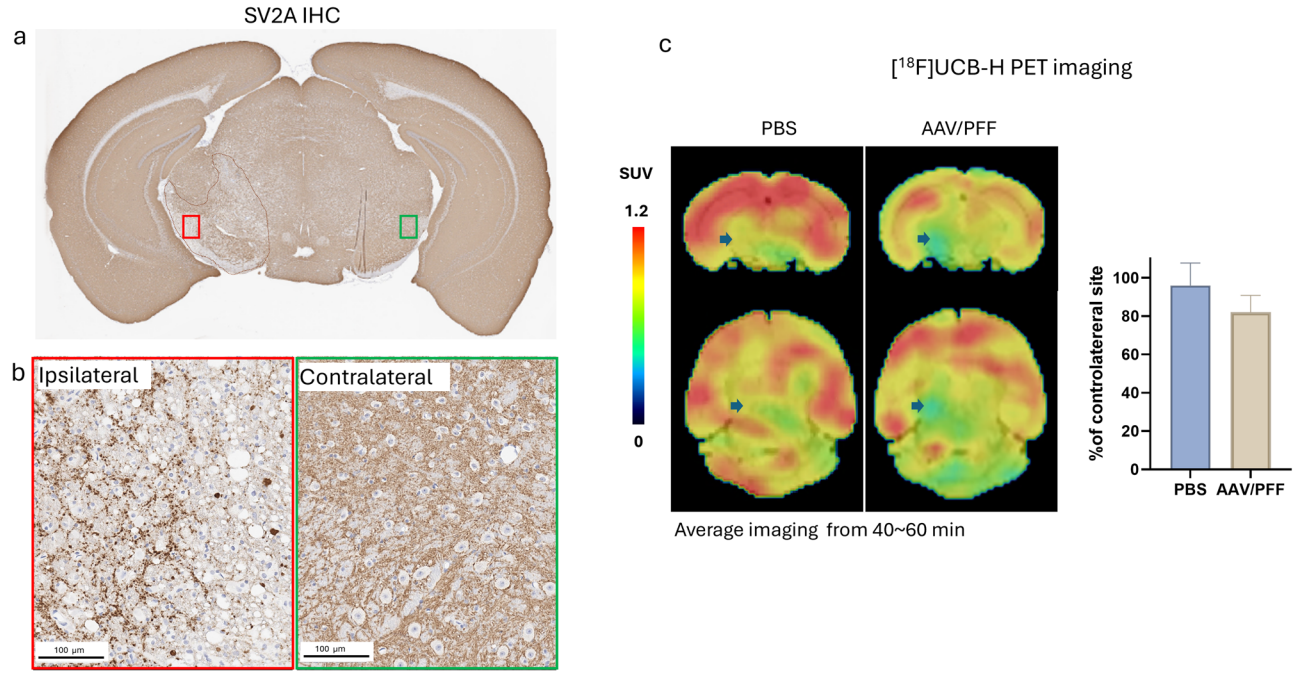

Fig. 5 | SV2A density reduction. Validated by SV2A IHC and PET imaging using [^{18}F]UCB-H. **a**, **b** SV2A IHC on brain sections across the SN. **c** [^{18}F]UCB-H PET tracer images and statistical analysis of ipsilateral SN (indicated by the blue arrow) for both PBS and AAV/PFF ($n = 3$).

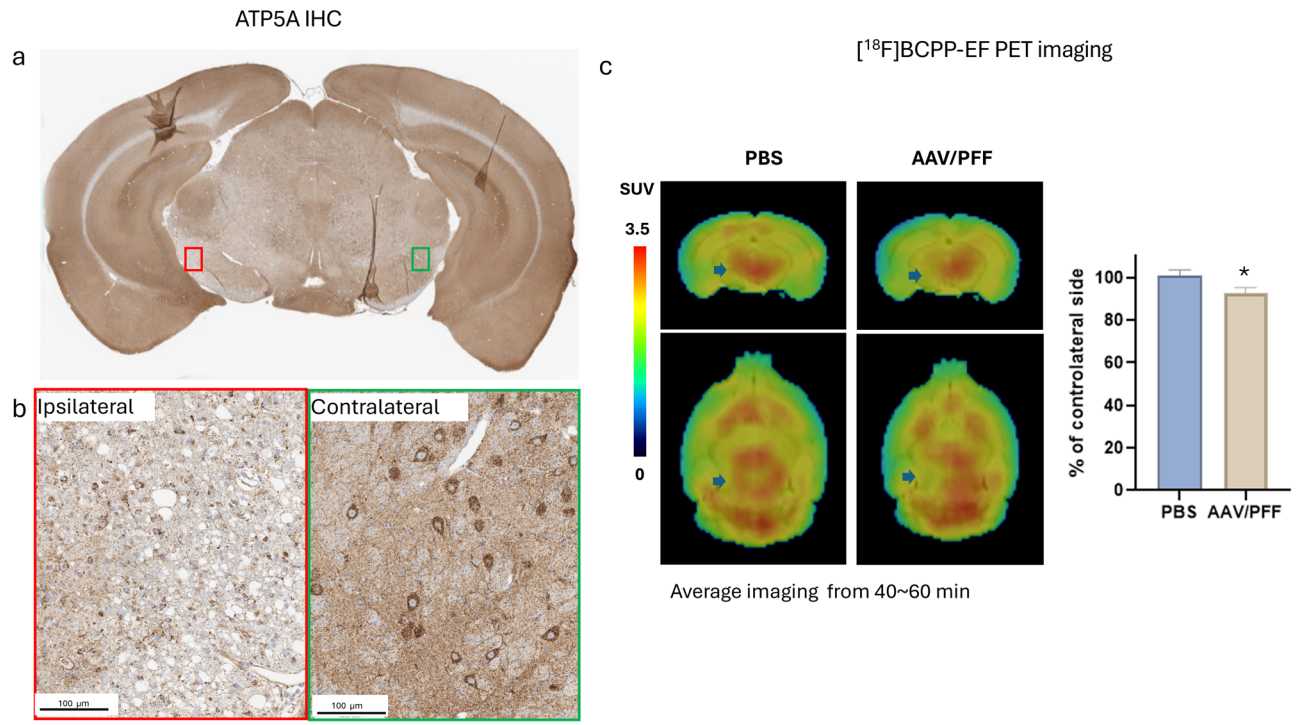

Fig. 6 | Mitochondrial dysfunction. Detected by ATP5A IHC (**a**, **b**) and MC-1 PET tracer images, along with statistical analysis of the injection site (indicated by the blue arrow) from PBS and AAV/PFF ($n = 3$, $^*P < 0.01$) (**c**).

In this study, we used human SN87 mutant α-syn PFFs together with AAV-carried human α-syn to generate rapid, reproducible pathology within the experimental window. The SN87 mutation accelerates fibrillization and seeding versus wild-type[23], and pathological α-syn deposits were detectable as early as 2 weeks with progressive accumulation through week 5 (Supplementary Fig. 2). The model effectively combines key features of the α-syn PFF and AAV-α-syn models, including the generation of toxic α-syn aggregates and Lewy body- and Lewy neurite-like inclusions induced by the SN87 PFF seeds, along with increased cellular levels of human α-syn driven by the AAV vector. Consequently, in response to pathological α-syn aggregation, the acute toxicity and DA neuron death were detected. The DA neuron intensity in the striatum is progressively reduced from 2 to 5 weeks post-injection. Neuroinflammation is recognized as a key factor in PD, which contributes to neurodegeneration by accelerating brain aging and

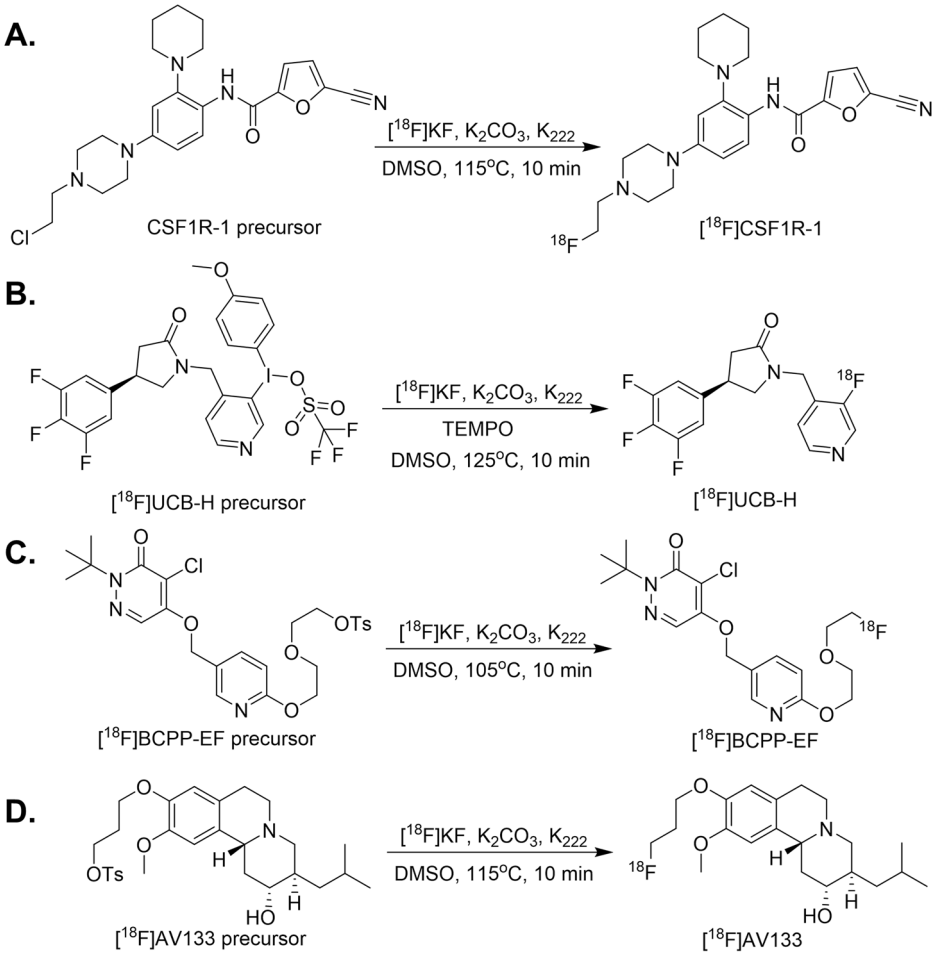

Fig. 7 | Radiolabeling reactions for PET ligands. **A** [^{18}F]JNJ-CSF1R-1, **B** [^{18}F]UCB-H, **C** [^{18}F]BCPP-EF, and **D** [^{18}F]AV-133.

inhibiting regeneration[24]. In this model, the increased microglial activation, assessed using Iba1, TREM2, and CSF1R staining, indicates a significant inflammatory response. SV2A, a synaptic protein, plays a vital role in the regulation of neurotransmitter release and is commonly used as a marker for synaptic density[25]. Notably, synaptic deficits are detected at a later time point (week 5) in this model. The loss of synaptic density is most pronounced in regions exhibiting pathological α-syn. Additionally, mitochondrial dysfunction is closely associated with genetic forms of PD, with several *PARK* genes being directly linked to impaired mitochondrial function and integrity[26]. ATP5A staining revealed substantial mitochondrial dysfunction in the same region where pathological α-syn is present. The interplay between synaptic deficits and mitochondrial dysfunction underscores the comprehensive nature of this model in capturing the multifaceted aspects of PD pathology.

The model's focal, rapidly developing pathology provides an excellent platform for PET ligand validation. In this study, several PET ligands were validated against IHC: DA neuron loss was detected by VMAT2 PET ligand [^{18}F]AV-133[27]; enhanced neuroinflammation was detected by [^{18}F]JNJ-CSF1R-1[20,21] PET imaging, which showed pattern of concordant with CSF1R IHC; synaptic density deficits were in vivo visualized and quantified by [^{18}F]UCB-H[28], a first generation of SV2A PET ligand. Additionally, [^{18}F]BCPP-EF, which targets mitochondrial complex I (MC-1), revealed a small but statistically significant reduction in mitochondrial integrity, underscoring PD-related mitochondrial dysfunction. These results support the use of this model for additional PET ligand validation, including the development of novel α-syn PET tracers, a highly desirable diagnostic tool for synucleinopathies.

The studies began at week 2 to comply with an Institutional Animal Care and Use Committee (IACUC)-mandated 2-week post-surgical recovery period. But the pathologies at the early time point were also validated. IHC at week 1 revealed robust human α-syn overexpression in the injected SN and striatum, with only sparse p-syn in the SN and no evidence of TH loss in the striatum (Supplementary Fig. 3). These findings further justify our study design. Comprehensive immunostaining was performed, including α-syn, p-syn, TH, CSF1R, and Iba1 across weeks 2–5 to confirm pathological α-syn accumulation, DA neuron changes, and neuroinflammation. These longitudinal data (Supplementary Fig. 2) were used to validate the model and to identify the most informative imaging windows for each PET tracer. While the manuscript cannot include the entire dataset of PET imaging data from this model, we plan to conduct expanded studies with additional PET scans to cover more time points and across varied AAV and PFF doses in the future. Longer follow-up time points will be incorporated to characterize the temporal progression from synaptic and mitochondrial dysfunction to subsequent neuronal death.

In conclusion, this accelerated and localized synucleinopathy mouse model provides a robust and reliable platform for studying PD pathologies and assessing potential PET ligands. Its capacity to replicate key PD features in a short timeframe makes it an invaluable tool for preclinical research and drug development. Future studies will focus on exploring its applications in evaluating novel PET ligands and PD therapies.

Methods

Animal model

All animal procedures adhered to the National Institutes of Health Guide for the Care and Use of Laboratory Animals and were approved by the IACUC of Johnson & Johnson. Adult male C57BL/6J mice (Strain #000664, 10 weeks old) were purchased from Charles River (Rockville, MD). Recombinant human α-syn (S87N) purification and the in vitro generation

of PFF were adapted from literatures[29,30]. Prior to intracranial injection, 1.5 μL of AAV1/2-CMV/CBA-human-A53T-α-syn WPRE-BGH-polyA (Charles River, 5×10^{12} gc/mL) was mixed 1:1 with sonicated recombinant human α-syn (S87N) PFF (1.5 μL, 2 mg/mL, Johnson & Johnson in Beerse, Belgium). Under 2% isoflurane anesthesia, 3 μL of mixed AAV/PFF or PBS was injected unilaterally (left, ipsilateral side) into the SN at the following coordinates: anteroposterior (AP), −3.0 mm (from bregma); mediolateral, −1.3 mm (from bregma); dorsoventral, -4.2 mm (from dura). PET imaging was conducted at selected time points post-injection. All mice were euthanized with CO_2, and fresh-frozen brain samples were collected at 2, 3, 4, and 5 weeks post-injection for pathological analysis. Each time point included $n = 3$ mice for both the PBS and AAV/PFF groups.

Radiosynthesis

Four tracers were radiolabeled in this study. The synthesis of ^{18}F-labeled tracers is illustrated in Fig. 7. [^{18}F]JNJ-CSF1R-1[21], [^{18}F]UCB-H[31], [^{18}F]BCPP-EF[32], and [^{18}F]AV-133[33] were synthesized as reported. The targets, radiochemical yields, specific activities, and radiochemical purities of the four tracers are presented in Supplementary Table 1.

Immunohistochemistry

To define the optimal imaging window for tracer validation, we first performed multiple IHCs to confirm progressive α-syn pathology, DA neuron loss, and neuroinflammation at 2, 3, 4, and 5 weeks post-surgery. Mouse brains were collected, immediately frozen in dry ice powder, and then stored at −80 °C. The frozen mouse brains were embedded in optimal cutting temperature compound and cut into 10 μm coronal sections that crossed the striatum or SN. To determine the expression of targets, IHC was performed. After fixing the sections in paraformaldehyde fixative solution (Alfa Aesar, MA), sections were incubated with 3% H_2O_2 solution to quench background fluorescence. Then sections were blocked with 10% goat serum in 0.01 M PBS for 1 h and incubated with primary antibodies overnight at 4 °C. The results were visualized by fluorescent secondary antibodies (ThermoFisher, CA) under an Axio Imager 2 microscope (Carl Zeiss, Germany) and STELLARIS Confocal Microscope (Leica, IL).

For signal-plex or multiplex staining, mouse brain sections were stained using TSA-Opal fluorescent detection reagents and antibodies. The staining was performed with a Leica Bond Rx autostainer (Leica, IL), followed by imaging on a Vectra Polaris™ Quantitative Pathology Imaging System (Akoya Biosciences, MA)[34]. Antibodies used in this study are listed in the Supplementary Table 2.

PET/CT imaging

PET/CT imaging protocols were developed based on preclinical literature[35]. An intravenous catheter was placed in each mouse prior to imaging. The animals were then positioned in the GNEXT preclinical PET/CT system (Xodus Imaging, CA, USA) on a custom three-dimensional (3D) printed mouse-hotel bed. The ligand was administered intravenously via catheter in a volume of 150 μL of isotonic saline, followed by an additional 50 μL of fresh saline. Whole-body imaging was conducted with a field of view (FOV) measuring 120 × 104 mm and an average spatial resolution of less than 1 mm at the center of the FOV. List-mode data were recorded for 60 min for all tested tracers, followed by acquisition of a reference CT image using the embedded microCT imaging system. PET images were reconstructed using a 3D-OSEM reconstruction algorithm, which corrected for attenuation and decay, resulting in an isotropic voxel size of 540 μm. The 25 re-binned frame rate consisted of intervals: 4 × 5 s, 4 × 10 s, 2 × 30 s, 5 × 120 s, 5 × 300 s, and 2 × 600 s. CT images were reconstructed with a 200 μm isotropic voxel size for anatomical co-registration and attenuation correction. During imaging, the animals were maintained under 1–2% isoflurane anesthesia in oxygen, with continuous monitoring of respiration and temperature using a setup from Small Animal Instruments (SAII Inc., Stony Brook, NY, USA). Image analysis was performed using PMOD software (version 4.4, PMOD Technologies LLC), and only data collected 40–60 min post-injection were extracted for analysis. A 3D ROI was defined using threshold segmentation to capture the response at the injection site in the AAV/PFF group, along with a corresponding symmetrical mirror region established as a contralateral control ROI for comparative analysis. In addition, A mouse T2-magnetic resonance template was aligned with the PET images, facilitating visual identification of the brain regions.

Statistical analysis

All statistical analyses were conducted using GraphPad Prism software version 9 (Prism, CA, USA). Data are presented as the mean ± standard deviation. An ordinary one-way ANOVA with multiple comparisons was employed to compare three or more groups, while comparisons between two groups were performed using a *t*-test. A P value of <0.05 indicates statistical significance.

Data availability

All data generated or analyzed during this study are included in this published article and its supplementary information files.

Received: 9 October 2025; Accepted: 12 January 2026;
Published online: 02 February 2026

References

1. Dickson, D. W. Parkinson's disease and Parkinsonism: neuropathology. *Cold Spring Harb. Perspect. Med.* **2**, https://doi.org/10.1101/cshperspect.a009258 (2012).
2. Visanji, N. P. et al. alpha-Synuclein-based animal models of Parkinson's disease: challenges and opportunities in a new era. *Trends Neurosci.* **39**, 750–762 (2016).
3. Negi, S., Khurana, N. & Duggal, N. The misfolding mystery: alpha-synuclein and the pathogenesis of Parkinson's disease. *Neurochem. Int.* **177**, 105760 (2024).
4. Yasuda, T., Nakata, Y. & Mochizuki, H. alpha-Synuclein and neuronal cell death. *Mol. Neurobiol.* **47**, 466–483 (2013).
5. Beal, M. F. Experimental models of Parkinson's disease. *Nat. Rev. Neurosci.* **2**, 325–334 (2001).
6. Khan, E., Hasan, I. & Haque, M. E. Parkinson's disease: exploring different animal model systems. *Int. J. Mol. Sci.* **24**, https://doi.org/10.3390/ijms24109088 (2023).
7. Mondal, R., Campoy, A. T., Liang, C. & Mukherjee, J. (18) F]FDG PET/CT studies in transgenic Hualpha-Syn (A53T) Parkinson's disease mouse model of alpha-synucleinopathy. *Front. Neurosci.* **15**, 676257 (2021).
8. Bjorklund, A. & Mattsson, B. The AAV-alpha-synuclein model of Parkinson's disease: an update. *J. Parkinsons Dis.* **14**, 1077–1094 (2024).
9. Daher, J. P. et al. Conditional transgenic mice expressing C-terminally truncated human alpha-synuclein (alphaSyn119) exhibit reduced striatal dopamine without loss of nigrostriatal pathway dopaminergic neurons. *Mol. Neurodegener.* **4**, 34 (2009).
10. Koprich, J. B., Kalia, L. V. & Brotchie, J. M. Animal models of alpha-synucleinopathy for Parkinson disease drug development. *Nat. Rev. Neurosci.* **18**, 515–529 (2017).
11. Ip, C. W. et al. AAV1/2-induced overexpression of A53T-alpha-synuclein in the substantia nigra results in degeneration of the nigrostriatal system with Lewy-like pathology and motor impairment: a new mouse model for Parkinson's disease. *Acta Neuropathol. Commun.* **5**, 11 (2017).
12. Faustini, G. et al. Synapsin III deficiency hampers alpha-synuclein aggregation, striatal synaptic damage and nigral cell loss in an AAV-based mouse model of Parkinson's disease. *Acta Neuropathol.* **136**, 621–639 (2018).
13. Wu, Q. et al. alpha-Synuclein (alphaSyn) preformed fibrils induce endogenous alphaSyn aggregation, compromise synaptic activity and enhance synapse loss in cultured excitatory hippocampal neurons. *J. Neurosci.* **39**, 5080–5094 (2019).

14. Chung, H. K., Ho, H. A., Perez-Acuna, D. & Lee, S. J. Modeling alpha-synuclein propagation with preformed fibril injections. *J. Mov. Disord.* **12**, 139–151 (2019).
15. Thakur, P. et al. Modeling Parkinson's disease pathology by combination of fibril seeds and alpha-synuclein overexpression in the rat brain. *Proc. Natl. Acad. Sci. USA* **114**, E8284–E8293 (2017).
16. Bjorklund, A., Nilsson, F., Mattsson, B., Hoban, D. B. & Parmar, M. A combined alpha-synuclein/fibril (SynFib) model of Parkinson-like synucleinopathy targeting the nigrostriatal dopamine system. *J. Parkinsons Dis.* **12**, 2307–2320 (2022).
17. Loane, C. & Politis, M. Positron emission tomography neuroimaging in Parkinson's disease. *Am. J. Transl. Res.* **3**, 323–341 (2011).
18. Hauer, K. O. et al. CSF markers of neuroinflammation, synaptic dysfunction and [(18)F]DOPA-PET in Parkinson's disease. *Parkinsonism Relat. Disord.* **139**, 108005 (2025).
19. Li, S. et al. Characteristics of the 18F-fluorodeoxyglucose ((18)F-FDG) and [(18)F] 9-fluoropropyl-(+)-dihydrotetrabenazine ((18)F-FP-DTBZ) positron emission tomography (PET) in patients with cognitive impairment in Parkinson's disease. *Clin. Radiol.* **89**, 107038 (2025).
20. Lee, H. et al. Synthesis and evaluation of a (18)F-labeled ligand for PET imaging of colony-stimulating factor 1 receptor. *Pharmaceuticals* **15**, https://doi.org/10.3390/ph15030276 (2022).
21. Salarian, M. et al. Evaluation of [(18)F]JNJ-CSF1R-1 as a positron emission tomography ligand targeting colony-stimulating factor 1 receptor. *Mol. Imaging Biol*. https://doi.org/10.1007/s11307-025-01991-9 (2025).
22. Abdelmotilib, H. et al. alpha-Synuclein fibril-induced inclusion spread in rats and mice correlates with dopaminergic Neurodegeneration. *Neurobiol. Dis.* **105**, 84–98 (2017).
23. Ohgita, T. et al. Intramolecular interaction kinetically regulates fibril formation by human and mouse alpha-synuclein. *Sci. Rep.* **13**, 10885 (2023).
24. Araujo, B. et al. Neuroinflammation and Parkinson's disease—from neurodegeneration to therapeutic opportunities. *Cells* **11**, https://doi.org/10.3390/cells11182908 (2022).
25. Rossi, R., Arjmand, S., Baerentzen, S. L., Gjedde, A. & Landau, A. M. Synaptic Vesicle Glycoprotein 2A: features and functions. *Front. Neurosci.* **16**, 864514 (2022).
26. Henrich, M. T., Oertel, W. H., Surmeier, D. J. & Geibl, F. F. Mitochondrial dysfunction in Parkinson's disease—a key disease hallmark with therapeutic potential. *Mol. Neurodegener.* **18**, 83 (2023).
27. Beauchamp, L. C. et al. Using (18)F-AV-133 VMAT2 PET Imaging to Monitor Progressive Nigrostriatal Degeneration in Parkinson Disease. *Neurology* **101**, e2314–e2324 (2023).
28. Warnock, G. I. et al. Evaluation of 18F-UCB-H as a novel PET tracer for synaptic vesicle protein 2A in the brain. *J. Nucl. Med.* **55**, 1336–1341 (2014).
29. Giasson, B. I., Murray, I. V., Trojanowski, J. Q. & Lee, V. M. A hydrophobic stretch of 12 amino acid residues in the middle of alpha-synuclein is essential for filament assembly. *J. Biol. Chem.* **276**, 2380–2386 (2001).
30. Luk, K. C. et al. Exogenous alpha-synuclein fibrils seed the formation of Lewy body-like intracellular inclusions in cultured cells. *Proc. Natl. Acad. Sci. USA* **106**, 20051–20056 (2009).
31. Warnier, C. et al. Enabling efficient positron emission tomography (PET) imaging of synaptic vesicle glycoprotein 2A (SV2A) with a robust and one-step radiosynthesis of a highly potent (18)F-labeled ligand ([(18)F]UCB-H). *J. Med. Chem.* **59**, 8955–8966 (2016).
32. Kaur, T. et al. Automated synthesis of (18)F-BCPP-EF 2-tert-butyl-4-chloro-5-6-[2-(2[(18)F]fluoroethoxy)-ethoxy]-pyridin-3-ylmethoxy-2H-pyridazin-3-one for imaging of mitochondrial complex 1 in Parkinson's disease. *Front. Chem.* **10**, 878835 (2022).
33. Zhu, L. et al. An improved radiosynthesis of [18F]AV-133: a PET imaging agent for vesicular monoamine transporter 2. *Nucl. Med. Biol.* **37**, 133–141 (2010).
34. Taube, J. M. et al. Multi-institutional TSA-amplified multiplexed immunofluorescence reproducibility evaluation (MITRE) study. *J. Immunother. Cancer* **9**, https://doi.org/10.1136/jitc-2020-002197 (2021).
35. Ni, R. Positron emission tomography in animal models of Alzheimer's disease amyloidosis: translational implications. *Pharmaceuticals* **14**, https://doi.org/10.3390/ph14111179 (2021).

Acknowledgements

This study was fully funded by Johnson & Johnson.

Author contributions

C. Xia: conceptualization, formal analysis, investigation, methodology, project administration, visualization, writing—original draft, writing—review and editing. HM Tsai: formal analysis, investigation, writing—original draft. SD Garcia: formal analysis, investigation. SL Liu: investigation. A. Matzeu: investigation. M Salarian: methodology. W Bruinzeel: investigation. AK Szardenings: conceptualization, writing—review and editing, and supervision.

Competing interests

The authors declare no competing interests.

Additional information

Supplementary information The online version contains supplementary material available at https://doi.org/10.1038/s44303-026-00138-x.

Correspondence and requests for materials should be addressed to Chunfang A. Xia.